OXFORD JOURNAL
OF STUDENT
SCHOLARSHIP

Influence of Iron-Series Transition Metal Centers on the Electrochemical Performance of BDC-Based Metal-Organic Frameworks for Energy Storage

Rana Qadeer Ul Hassan
ranaqadeer1008@gmail.com

ABSTRACT

The transition towards sustainable energy systems signified electrochemical energy storage technologies; the electrode materials of these devices are of key importance. Metal-Organic frameworks (MOFs) have emerged as a potential candidate as electrode material for these devices due to their tunability and electrochemical versatility. A systematic understanding of how metal centre selection has an effect on the properties of electrode material is incomplete. This review addresses this gap by comparing iron series transition metals (Fe, Co, Ni, Mn) with the carboxylate ligand framework (1,4-benzenedicarboxylate) for applications in lithium-ion battery and supercapacitors. Analysis of a normalized performance data reveals that trimetallic system (CoCuNi-BDC/NF) achieve exceptional specific capacitance (2891 F g^{-1}) while monometallic frameworks show superior cyclic retention. Co-BDC (powder) maintained 85% retention after 2000 cycles. In lithium-ion battery, thermally activated Mn-1,4-BDC@200 shows the highest normalized capacity (974 mAh g^{-1} at 100 mA g^{-1}) while Fe-based MOFs require conductive material (such as reduced graphene oxide) to overcome its electronic limitations. These findings show the significance of metal centre and how it contributes to the electrochemical properties.

1. INTRODUCTION

In recent years, with the rapid increase in the fossil fuel crisis and environmental pollution the need for clean, safe, renewable, and sustainable energy storage and conversion technologies is increased [1-5]. To address these challenges, strategies devised aim at mitigating the greenhouse effect and conserving diminishing fossil resources, both of which are central to the transition toward green energy systems [6]. Although renewable sources such as wind, solar, and tidal energy offer considerable potential, their intermittent nature and uneven geographical distribution limit their direct and widespread deployment. Consequently, the development of renewable, environmentally benign, and highly efficient energy-storage and conversion systems has become a major focus within the scientific community [7-11]. Among these systems, rechargeable batteries and high-performance supercapacitors have emerged as the most extensively investigated electrochemical energy-storage (EES) devices due to their ability to meet diverse

performance demands [12-15]. Within this context, electrode materials, used in rechargeable batteries and supercapacitors play an essential role and their optimization has become a dynamic area of research looking to enhance the energy-storage capabilities in both batteries and supercapacitors [16].

Metal Organic Frameworks (MOFs) due to their tunability and exceptional physiochemical properties emerged as an important class of materials for electrochemical energy storage (EES) [17, 18]. MOFs, also known as coordination polymers are synthetic crystalline materials made up of ions or clusters of ions (metal centers) that are connected via organic linkers (usually containing imidazolate or carboxylate groups) forming 3D structures. The MOFs are constructed through a "*node-spacer*" strategy which allows to produce frameworks that are highly porous, structurally ordered, and capable of accommodating large accessible surface areas, all of which make them high-performance EES materials. There are different types of MOFs, among them, MOFs incorporating iron-series transition metals (Fe, Mn, Co, Ni) are particularly attractive due to advantages such as natural abundance, high storage capacity, low cost, environmental friendliness, safety, and nontoxicity. In addition, these metals have similar electron configurations, providing comparable electrochemical behavior and numerous coordination sites for organic ligands, thereby supporting the rational design and synthesis of new MOF architectures for energy-storage applications [19, 20].

There has been great progress in designing MOFs for electrochemical energy storage but the existing research remains highly fragmented. The articles reported so far study Fe-, Co-, Ni-, or Mn-based MOFs under distinct synthetic conditions, morphologies, and ligand environments. There is lack of uniformity which makes it difficult to understand the intrinsic role of the metal node, leaving uncertainty about how the metal center itself governs redox activity, electronic conductivity, and long-term structural stability. To address this gap, the present study focuses on comparing MOFs derived from iron, cobalt, nickel, and manganese within a consistent carboxylate-based ligand (1,4 Benzene dicarboxylic acid) framework. By narrowing the scope to systems sharing similar coordination chemistry, this review aims to establish clearer relationships between metal identity, framework structure, and electrochemical performance, thereby providing a more reliable basis for understanding how the choice of metal governs the performance of the MOF-based electrode materials.

2. LITERATURE REVIEW

2.1. Charge Storage Mechanism

The performance of electrochemical energy-storage devices depends strongly on how charge is stored at the electrode level. Different charge-storage mechanisms lead to clear differences in energy density, power output, and cycling stability, making their understanding essential when designing efficient systems [21]. In practice, charge storage can be divided into two main categories. In non-faradaic systems, charge is stored through the physical separation of ions and electrons at the electrode-electrolyte interface, without involving chemical reactions. By contrast, faradaic charge storage arises from electron transfer processes that occur within the electrode material itself.

The electrical double-layer (EDL) capacitance involve non-faradaic behaviour where charge is stored by the electrostatic ion adsorption at the interface of electrode and electrolyte without involving redox reactions [18]. In this process, the reversible electrosorption of ions on the accessible external and internal surfaces increases the surface area and pore accessibility, both of which are key contributors in the performance of particular material. This mechanism does not require any structural rearrangements, therefore EDL-based supercapacitors show ultrafast charge-discharge capability, high power density, and excellent long-term cycling stability, often exceeding 100,000 cycles [21].

Faradaic processes support charge storage in batteries, where redox reactions are accompanied by ion insertion, intercalation, or structural transformations within the electrode material. These reactions provide significantly higher specific capacities and energy densities than EDL mechanisms but are constrained by solid-state diffusion and lattice changes that slow overall kinetics [21-23]. In this context, pseudocapacitance occupies an intermediate regime: although it relies on faradaic reactions, these redox events occur rapidly at or near the surface, allowing pseudocapacitive materials to store 5-10 times more charge than EDLCs while maintaining high power performance [18]. This hybrid behavior enables pseudocapacitors to bridge the gap between batteries and capacitors, offering a balance of high energy and high power that is highly desirable for next-generation energy-storage devices.

2.2. Coordination Chemistry and Structural Characteristics of Iron-Series Metal Centers in MOFs

The coordination chemistry plays a vital role in the synthesis of metal organic framework; it is significant in understanding the structural and electrochemical properties of these materials. MOFs are made up of metal ions or clusters that act as nodes, and these are linked with organic ligands to generate extended crystalline three dimensional structures with well-define porosity and tunable geometries [24]. The flexibility of these structures allows the adjustments to framework chemistry, stability, particle size by varying metal-ligand combinations and synthetic conditions [25-27]. This tunability makes MOFs particularly adaptable for applications requiring precise control over structural and functional attributes.

These structural features are especially valuable for electrochemical energy storage, where porosity, accessible surface area, and robust coordination networks strongly influence performance. High internal surface area and hierarchical pore architectures facilitate efficient charge transport by shortening ion-diffusion pathways, an essential requirement for fast charge-discharge operation [28]. MOFs also exhibit high thermal and chemical stability and allow more effective utilization of metal centres than purely organic materials, while their morphology and pore environment can be tailored by appropriate selection of metal ions and linker chemistry to optimize redox accessibility and ion mobility [29, 30].

Among these systems, MOFs incorporating Fe, Co, and Ni have emerged as especially promising candidates for high-performance electrode materials due to the versatile coordination environments enabled by their partially filled d-orbitals. Fe-based MOFs typically form periodic network structures in which isolated Fe sites, high porosity, and large surface area combine to provide abundant active centres for electrochemical reactions. Additionally, iron-series metals are particularly attractive in this context, their shared $3d^{6-8}4s^2$ electron configurations, which provide multiple accessible oxidation states and

numerous coordination sites, promoting strong metal-ligand interactions and enabling the formation of frameworks with well-defined active sites and uniform metal distribution [19, 31, 32].

Co-based MOFs often crystallize into porous architectures with excellent redox accessibility and enhanced electronic characteristics associated with cobalt centres, properties that support strong performance in energy-related applications. Ni-based MOFs are widely investigated for supercapacitor electrodes because they can form under mild conditions and possess organized pore networks enriched with Ni^{2+}/Ni^{3+} redox sites that contribute directly to pseudocapacitive behaviour [32]. Collectively, the structural diversity and redox flexibility of iron-series transition-metal MOFs provide a versatile platform for designing materials that balance ion transport, structural stability, and electrochemical activity-parameters central to advanced energy-storage systems.

2.3. Charge Conduction in MOFs

The power performance of electrochemical energy-storage devices is governed by the electrical conductivity of the electrode material, since the rate of charge transfer depends on how efficiently electrons can move through the structure [18]. In most conventional MOFs, the presence of carboxylate linkers leads to the formation of strong ionic metal-oxygen bonds, which confer structural stability but typically result in poor intrinsic conductivity [33, 34]. Despite this limitation, recent advances in MOF design have enabled the development of conductive frameworks by tuning their structures and electronic properties [35, 36].

Charge transport in MOFs generally proceeds through either hopping or band-type mechanisms, depending on the degree of electronic coupling between sites. In systems where redox-active centers are spatially isolated and interactions are weak, electrons move via thermally activated hopping between localized states, a process characteristic of disordered or weakly connected frameworks [37]. By contrast, when adjacent sites exhibit strong orbital overlap-similar to that observed in crystalline inorganic conductors-extended energy bands can form, allowing electrons to delocalize and move more freely through the lattice [37, 38]. Alignment of the electronic states between neighboring nodes further enhances this delocalization and can significantly improve bulk conductivity [37, 39].

Several intrinsic features of MOFs, however, inhibit efficient electron transport, creating a tension between structural advantages and conductive limitations. The ionic character of metal-ligand bonds tends to localize charge carriers, while the high porosity that benefits ion accessibility often reduces orbital overlap and further restricts electron mobility [37, 40]. As a result, porosity and conductivity frequently compete within a single framework. To address these limitations, two primary strategies have emerged. In the through-bond approach, conjugated linkers and metal nodes create continuous coordination pathways that facilitate electron flow [37]. In the through-space approach, overlapping π-systems enable electrons to move between stacked aromatic units, generating conductive pathways independent of metal-ligand bonds [39, 41-43].

Energy-storage devices prefer different material characteristics; therefore, the selection of an appropriate conduction strategy depends on the desired electrochemical application. Each property imparts different benefits for example high porosity is helpful in those systems that usually store or convert molecular species such as, lithium-sulfur or lithium-oxygen batteries, where pore volume promotes efficient reactant confinement and transport. In such cases, maintaining robust coordination networks that support through-bond conduction may be preferable to highly π-stacked structures that emphasize through-space pathways [44]. Overall, understanding how electronic, chemical, and structural features contribute to conduction is essential for designing MOFs that balance porosity, stability, and conductivity for optimal energy-storage performance.

2.4. Applications in Supercapacitors

Supercapacitors are a promising type of electrochemical energy storage devices that is present in between the traditional capacitors and current rechargeable capacitors [45]. The main constituents are electrodes, separators and electrolytes, out of these the electrode material is of prime importance as it directly relates with the electrochemical performance of these devices [46]. The ongoing research on the electrode materials aimed to increase their electrochemical active surface area (ECASA), for this purpose MOFs are potential candidates [32]. Herein, we discuss Mn, Fe, Co, Ni MOFs incorporating BDC ligand reported for supercapacitors applications.

2.4.1. Co-BDC MOF

Sneha Tomar and Vinod Kumar Singh [47] synthesized metal-organic frameworks (MOFs) using cobalt metal ions with benzenedicarboxylic acid (bdc) as a common ligand. Structural characterizations indicate that Co-bdc MOF is composed of three-dimensional non uniform colloids possessing good crystalline structure. The Co-bdc MOF exhibited a maximum specific capacitance of 368 F/g at the current density of 1 A/g, 0.09 Ω ~ solution resistance and better cycling performance by retaining 85 % of its capacity after 2000 charge-discharge cycles. Conclusively, the Co-bdc MOF demonstrated superior specific capacitance, lower resistance, and enhanced cyclic stability in 3 M KOH electrolyte system.

2.4.2. Mn-BDC MOF

Shashank Sundriyal and Sunita Mishra [48] utilized Mn-BDC based coordination polymers due to their low toxicity and low cost to synthesize Mn-MOF. Structural Characterization shows that Mn-bdc MOF has a homogeneous laminar structure which is bounded loosely and has mesoporous nature. Cyclic Voltammetry shows highest specific capacitance value obtained for Mn-BDC electrode is 166.4 F/g at a scan rate of 1 mV/s, current densities ranging from 0.5 to 10 A/g and nyquist plot in shows the Rs and Rct values of 34.2 Ω and 10.2 Ω respectively. The fabricated symmetrical supercapacitor shows enormous electrochemical performance in terms of high specific capacitance, energy and power density while retaining a specific capacitance of 98 % after 2000 charge-discharge cycles. These results confirm the superiority of Mn-BDC based symmetrical supercapacitors for next generation practical supercapacitor applications.

2.4.3. Two-dimensional bimetallic Fe/M- (Ni, Zn, Co and Cu) MOF

Ravi Nivetha utilized [49] two-dimensional bimetallic Fe/M- (Ni, Zn, Co and Cu) metal-organic frameworks due to their synergistic effects and high electrocatalytic performance to synthesize 2D Fe/M-BDC MOFs. Structural Characterization shows that Fe/Ni-BDC and Fe/Zn-BDC display typical 2D interconnected sheet-like structures with lateral sizes around 50 to 100 nm. The BET surface areas of Fe/Ni-BDC and Fe/Zn-BDC were 130.77 and 66.14 m^2/g respectively, with mesoporous nature and mean pore sizes of 5.5 nm and 10.1 nm. Cyclic Voltammetry shows the highest specific capacitance values obtained for Fe/Ni-BDC and Fe/Zn-BDC electrodes are 1190.88 F/g and 633.21 F/g at a scan rate of 1 mV/s, respectively. GCD measurements were conducted at current densities ranging from 0.5 to 10 A/g. The Nyquist plot shows the charge transfer resistance (Rct) values of Fe/Ni-BDC and Fe/Zn-BDC are 9.145 Ω and 9.98 Ω, respectively. The Fe/Ni-BDC and Fe/Zn-BDC electrodes exhibited capacitance retention of 93.7% and 83.5% after 5000 cycles at 2 M KOH. These results confirm the superiority of Fe/M-BDC based electrodes for energy storage applications.

2.4.4. CoCuNi-BDC MOF

Nurul Khairiyyah Mohd Zain [50] utilized triple cation metal-organic frameworks due to their robust structure with high surface area and open metal center sites which easily undergo reversible redox reactions to synthesize CoCuNi-bdc/NF MOF and its single metal counterparts (Co-bdc/NF, Cu-bdc/NF, and Ni-bdc/NF). Structural Characterization shows that CoCuNi-bdc/NF displays worm-like nanofibers of diameter ~80-100 nm with large aspect ratio, while Co-bdc/NF shows uniformly distributed nanofiber network bundled on edges of plate-like structures with average width of ~500 nm. Cu-bdc/NF exhibits similar morphology to CoCuNi-bdc/NF but with slightly fused fibers, and Ni-bdc/NF displays mixed structures consisting of smooth and dense sheet-like and petal-like morphologies with average length of ~3.4 μm and width of ~300 nm. Cyclic Voltammetry shows CoCuNi-bdc/NF exhibits redox peaks at 0.34 and 0.19 V (vs. Ag/AgCl) demonstrating pseudocapacitive behavior. GCD measurements show the highest specific capacity obtained for CoCuNi-bdc/NF electrode is 321.3 mA h g^{-1} (~2892 F g^{-1}) at a current density of 1 A g^{-1}, which is superior to Co-bdc/NF (~208.2 mA h g^{-1}; ~1874 F g^{-1}), Cu-bdc/NF (~171.3 mA h g^{-1}; ~1542 F g^{-1}), and Ni-bdc/NF (~143.3 mA h g^{-1}; ~1290 F g^{-1}). Current densities ranged from 1 to 40 A g^{-1}, and the Nyquist plot shows the Rs values of CoCuNi-bdc/NF, Co-bdc/NF, Cu-bdc/NF, and Ni-bdc/NF are 0.28 Ω, 0.31 Ω, 0.37 Ω, and 0.47 Ω, respectively. The internal resistance values are 0.54 Ω, 0.56 Ω, 0.66 Ω, and 0.55 Ω for CoCuNi-bdc/NF, Co-bdc/NF, Cu-bdc/NF, and Ni-bdc/NF, respectively. The CoCuNi-bdc/NF electrode retained ~77% capacity at 10 A g^{-1} and ~59% at 40 A g^{-1}, with ~76% capacity retention (186 mAh g^{-1}) after 1000 cycles at 10 A g^{-1}. These results confirm the superiority of CoCuNi-bdc/NF electrode as a promising electrode material for supercapacitor applications [50].

2.5. Applications in Lithium-ion batteries (LiB)

Lithium-ion batteries (LiB) are beneficial because of their high energy density, superior cycling performance, wide operating-temperature range, rapid charging and discharging, long service life and high charging efficiency. These are high-performance batteries, which has made them significant for portable electronic devices and wide-scale applications [51]. MOFs are promising candidates for LIBs

due to their exceptional structural characteristics [52]. The inner cavities of MOFs can speed up the Li-ion transfer, which make them suitable as electrode materials [53]. Improvement in the surface morphology of MOFs gives a more suitable LIB reaction space which will improve the surface area that is needed for optimal electrolyte exposure [32, 54].

2.5.1. Mn-BDC Li-batteries

Huiping Hu [55] utilize Mn-based MOFs due to their low toxicity, low cost, and facile synthesis method to synthesize Mn-1,4-benzenedicarboxylate (Mn-1,4-BDC) MOF and its thermally activated form Mn-1,4-BDC. Structural Characterization shows that Mn-1,4-BDC has a loose homogeneous laminar structure with monoclinic crystalline framework of MnO_6 octahedral geometry. After thermal treatment at 200°C, the bulky laminar structure fragmented into small pieces in Mn-1,4-BDC@200, with elements C, O, and Mn uniformly distributed. The BET surface areas of Mn-1,4-BDC and Mn-1,4-BDC@200 are 5.563 $m^2\ g^{-1}$ and 6.135 $m^2\ g^{-1}$, respectively, with mesopores (3 to 12 nm) and macropores (50-110 nm). Cyclic Voltammetry shows two cathodic peaks at 0.67V and 0.19V in the first reduction process, and one anodic peak at 1.11V, indicating lithium ion insertion/extraction reactions at a scan rate of 0.2 mV s^{-1} in the voltage range of 0.01-3.0 V. GCD measurements show the highest reversible lithium storage capacity obtained for Mn-1,4-BDC@200 electrode is 974 mA h g^{-1} after 100 cycles at a current density of 100 mA g^{-1}, which is superior to Mn-1,4-BDC (725.2 mA h g^{-1}). The initial discharge and charge capacities are 1746 and 706.4 mA h g^{-1}, respectively, corresponding to an initial coulombic efficiency of 40.5%. Current densities tested ranged from 100 to 1000 mA g^{-1}, with reversible capacities of 870.6, 740.1, 683, 530, and 435 mA h g^{-1} at 100, 200, 500, 800, and 1000 mA g^{-1}, respectively. The Nyquist plot shows that charge-transfer resistance (Rct) is significantly reduced after heat treatment. Mn-1,4-BDC@200 maintained a coulombic efficiency above 98% after initial cycles and retained excellent capacity with nearly 100% coulombic efficiency after 10 cycles. These results confirm the superiority of Mn-1,4-BDC@200 as one of the best lithium storage materials among reported MOF-based anodes for lithium-ion battery applications.

2.5.2. Co-BDC Li-Batteries

Lei Gou [56] utilize 3D metal-organic frameworks to synthesize $Co_2(OH)_2$BDC (BDC=1,4-bdc) MOF. Structural Characterization shows that $Co_2(OH)_2$BDC has a rectangular-parallelepiped shape microcrystal morphology with well-crystallinity, though these microcrystals aggregated together into large bulk grains. Cyclic Voltammetry shows a cathodic peak at +0.7 V and an anodic band at +1.3 V in the first cycle at a scan rate of 0.3 mV s^{-1} in the voltage range of 0.02-3.0 V, attributed to the lithiation and delithiation processes. Galvanostatic charge-discharge measurements show the highest reversible capacity obtained for $Co_2(OH)_2$BDC electrode is approximately 650 mA h g^{-1} at a current density of 50 mA g^{-1} after 100 cycles within the voltage range of 0.02-3.0 V. The first discharge and charge capacities are 1385 and 1005 mA h g^{-1}, respectively, with a coulombic efficiency of 72.8%. In the second cycle, discharge and charge capacities are 792 and 733 mAh g^{-1}, respectively, with a coulombic efficiency of 92.5%. Current densities ranging from 50 to 500 mA g^{-1} were tested, delivering capacities of 540 mA h g^{-1} at 100 mA g^{-1}, 470 mA h g^{-1} at 250 mA g^{-1}, and 210 mA h g^{-1} at 500 mA g^{-1}. The coulombic efficiency was found to be ≥99% after 10 cycles. When the current density returned to 50 mA g^{-1}, the capacity recovered to 630 mA h g^{-1}

after 60 cycles. These results confirm the superiority of $Co_2(OH)_2BDC$ showing excellent cycling stability, enhanced specific capacity, and better rate capability compared with other reported benzenedicarboxylate based MOFs for lithium-ion battery anode applications.

2.5.3. Fe-based MOFs

Fe-based MOFs have been widely explored as electrode materials for lithium-ion batteries (LIBs) due to their strong structural stability and favorable redox activity, which together support efficient Li^+ storage [57-61]. Despite these advantages, their practical application remains limited by intrinsically low electrical conductivity, a factor that contributes to poor cycling performance in LIB systems. To mitigate this limitation, conductive additives such as graphene have been incorporated into MOF structures. Graphene offers exceptionally high electrical conductivity, which enhances electron transport within the electrode, while its porous and flexible architecture helps buffer the mechanical stress and volume variations that occur during repeated lithiation and delithiation, thereby reducing electrode pulverization and improving cycling stability [62].

Building on these advantages, Yan Jin and co-workers [63] prepared Fe-MOF/reduced graphene oxide (RGO) composites via a solvothermal method to achieve more reversible Li^+ storage. In this system, the pristine Fe-MOF crystallized into uniform octahedral particles with sizes ranging from 0.5 to 1.0 μm, and SEM analysis confirmed that these particles were effectively wrapped by two-dimensional RGO nanosheets. Electrochemical behavior was examined through cyclic voltammetry recorded between 0.01 and 3.0 V at a scan rate of 0.05 mV s^{-1}. During the initial cycle, Fe-MOF, Fe-MOF/RGO (5%), and Fe-MOF/RGO (10%) all showed a cathodic peak near 0.8 V and a broad anodic peak around 1.05 V, corresponding to lithium extraction. Notably, the Fe-MOF/RGO (10%) composite exhibited an additional anodic feature near 1.85 V, indicating modified redox behavior due to graphene incorporation. The first discharge/charge capacities for Fe-MOF, Fe-MOF/RGO (5%), and Fe-MOF/RGO (10%) were 2213/786, 2055.9/891.1, and 1889.9/750 mA h g^{-1}, respectively, yielding initial coulombic efficiencies of 35.5%, 43.3%, and 39.7%. These results highlight that integrating appropriate amounts of graphene can significantly improve the reversibility and overall electrochemical performance of Fe-based MOF electrodes.

3. METHODOLOGY

The data set analyzed in this review paper has been collected from the articles of peer reviewed journal through established scientific databases. For supercapacitor and lithium-ion battery applications, the electrochemical parameters has been recorded in the same units and experimental conditions as they were original reported in the publications.These datasets are presented in the table 1 and and table 2 for supercapacitor and lithium-ion battery respectively. As the dataset has been reported in different units and under different conditions, so direct comparison can not be made. In order to make the data comparable, the normalization strategy has been employed. For supercapacitor electrodes, reported capacities expressed in mAh g^{-1} were converted to specific capacitance (F g^{-1}) using a standard electrochemical conversion formula and the values reported in the same units have been reported as it is in Table 3. For

lithium-ion battery, the specific capacities were normalized to common power density of 100 mA/g using the formula and normalized dataset has been reported in Table 4. The resulting dataset has been used for making comparison and visual representations, the plots have been created using python.

4. RESULTS

The dataset collected from different articles has been reported in the Table 1 and Table 2 for supercapacitor and lithium-ion battery applications alongwith their experimental conditions and electrochemical conditions. The raw dataset already shows clear qualitative differences in performance between MOFs with different metal centers, even under the same ligand environment, which suggests that the metal center has a strong effect on electrochemical performance. However, because the dataset contains different testing conditions such as voltage windows, current densities, cycle counts, and reported units, these raw values cannot be directly compared on a quantitative basis; a normalization step, described below, is required before meaningful numerical comparisons can be made.

Table 1: Transition Metals MOFs with BDC ligand as electrode materials for Supercapacitor Application

MOF System	Metal Center(s)	Electrolyte	Voltage Window (V)	Specific Capacitance / Capacity	Test Condition (Scan Rate / Current Density)	Cycles	Retention (%)	Electrode Type	Ref.
Fe/Ni-BDC	Fe, Ni	2 M KOH	-0.2 to 0.25	**1190.88 F/g**	1 mV/s (CV)	5000	93.70%	3-electrode	[49]
Fe/Zn-BDC	Fe, Zn	2 M KOH	-0.2 to 0.25	**633.21 F/g**	1 mV/s (CV)	5000	83.50%	3-electrode	[49]
CoCuNi-BDC/NF	Co, Cu, Ni	6 M KOH	0-0.40	**321.3 mAh/g** (≈2892 F/g)	1 A/g	1000	76.20%	3-electrode on Ni-foam	[50]
Co-BDC/NF	Co	6 M KOH	0-0.40	**208.2 mAh/g** (≈1874 F/g)	1 A/g	1000	79.40%	Ni-foam	[50]
Cu-BDC/NF	Cu	6 M KOH	0-0.40	**171.3 mAh/g** (≈1542 F/g)	1 A/g	1000	79.70%	Ni-foam	[50]
Ni-BDC/NF	Ni	6 M KOH	0-0.40	**143.3 mAh/g** (≈1290 F/g)	1 A/g	1000	81.90%	Ni-foam	[50]
Co-BDC (powder)	Co	3 M KOH	-0.5 to 0.0	**368 F/g**	1 A/g	2000	85%	3-electrode	[47]

Mn-BDC	Mn	1 M Na_2SO_4	-0.2 to 0.8	**177.9 F/g**	0.5 A/g (GCD)	-	-	3-electrode	[48]
Mn-BDC (CV)	Mn	1 M Na_2SO_4	-0.2 to 0.8	**166.4 F/g**	1 mV/s	-	-	3-electrode	[48]
Mn-BDC (Symmetric Devices)	Mn	-	-	**-**	-	2000	98%	Symmetric (2-electrode)	[48]

Table 2: Transition Metals MOFs with BDC ligand as electrode material for Lithium ion batteries (LiB)

MOF System	Metal Center(s)	Electrolyte	Voltage Range (V vs Li/Li^+)	Discharge Capacity (mAh/g)	Charge Capacity (mAh/g)	Current Density	Cycles	CE (%)	Ref.
Mn-1,4-BDC @200	Mn	1 M $LiPF_6$ in EC-DEC-EMC (1:1:1)	0.01-3.0	**1746 (1st discharge)**	**706.4 (1st charge)**	100 mA/g	1	40.50 %	[55]
Mn-1,4-BDC @200 (100 cycles)	Mn	Same as above	0.01-3.0	**974**	~974	100 mA/g	100	>98% (after 10 cycles)	[55]
Mn-1,4-BDC (untreated)	Mn	1 M $LiPF_6$ (EC-DEC-EMC)	0.01-3.0	**1548 (1st discharge)**	**575.2 (1st charge)**	100 mA/g	1	37.15 %	[55]
Mn-1,4-BDC (100 cycles)	Mn	Same	0.01-3.0	**725.2**	~725	100 mA/g	100	>98% (after 10)	[55]
$Co_2(OH)_2BDC$ (1^{st} cycle)	Co	1 M $LiPF_6$ in EC:DMC (1:1)	0.02-3.0	**1385 (1st discharge)**	**1005 (1st charge)**	50 mA/g	1	72.80 %	[56]
$Co_2(OH)_2BDC$ (2nd cycle)	Co	Same	0.02-3.0	**792**	**733**	50 mA/g	2	92.50 %	[56]

$Co_2(OH)_2BDC$ (100 cycles)	Co	Same	0.02-3.0	**650**	~650	50 mA/g	100	≥99%	[56]
Fe-MOF	Fe^{3+}	1M $LiPF_6$ in FEC/EMC/DMC (1:1:1 v/v)	0.01-3.0 0 V	2213	786	500 mA/g	200	35.5%	[63]
Fe-MOF/RGO (5%)	Fe^{3+}	Same	0.01-3.0 0 V	2055.9	891.1	500 mA/g	200	43.3%	[63]
Fe-MOF/RGO (10%)	Fe^{3+}	same	0.01-3.0 0 V	1889.9	750	500 mA/g	200	39.7%	[63]

Note: For the Mn-1,4-BDC and $Co_2(OH)_2BDC$ entries, separate rows report first-cycle and 100-cycle capacities. For the Fe-MOF entries, the listed discharge/charge capacities are first-cycle values; the "200" in the Cycles column refers to the total number of charge–discharge cycles over which the source study evaluated these electrodes, not the capacity at cycle 200.

5. ANALYSIS AND DISCUSSION

The dataset reported in table 1 and table 2 has been normalized in the following way for supercapacitors and lithium-ion batteries.

For Supercapacitors

There are two normalization strategies that have been employed for the normalization of supercapacitor data set. First of all the values of capacitance has been brought to same unit (F/g), those values which have already been in F/g has been noted as it is, while the rest of the values have been converted by using the following formula

$$\boldsymbol{C_s(\mathrm{F/g}) = \frac{\mathrm{Capacity(mAh/g)} \times 3600}{\Delta V}}$$

Worked example: For Co-BDC/NF, the reported specific capacity is 208.2 mAh g^{-1} over a voltage window (ΔV) of 0.40 V. Applying Cs (F/g) = Capacity (mAh/g) × 3.6 / ΔV gives Cs = (208.2 × 3.6) / 0.40 = 749.5 / 0.40 ≈ 1874 F/g, matching the value reported in Table 1 and carried forward in Table 3.

In this formula, *Cs* **(F/g)** is Specific capacitance in Farads per gram, which is the standard unit for supercapacitors, **Capacity (mAh/g)** is Specific capacity in milliampere-hours per gram and is the potential window (voltage difference) over which charge and discharge occurs. The second normalization strategy which has been employed to normalize the data set for supercapacitor is normalizing the cycling retention data to per 1000 cycles which has been done using following formula

$$\boldsymbol{R_{1000}} = (\boldsymbol{R}_{\text{reported}})^{\boldsymbol{1000/n}}$$

Table 3 is showing the normalized capacitance and retention values for supercapacitor applications.

Table 3: Normalized Data for Supercapacitors

MOF	Normalized C (1 A/g)	R_{1000}	Notes
Fe/Ni-BDC	**1190.88 F/g**	0.987	highest bimetallic
Fe/Zn-BDC	**633.21 F/g**	0.965	moderate stability
CoCuNi-BDC/NF	**2892 F/g**	0.762	highest overall
Co-BDC/NF	**1874 F/g**	0.794	strong pseudocapacitance
Cu-BDC/NF	**1542 F/g**	0.797	similar to Co
Ni-BDC/NF	**1290 F/g**	0.819	higher stability
Co-BDC (powder)	**368 F/g**	0.922	very stable
Mn-BDC	**222 F/g**	0.990	lowest capacitance; R_{1000} computed from 98% @ 2000 cycles

The comparative bar chart (Figure 1) which has been made using the normalized dataset (Table 3) highlights a strong dependence of specific capacitance on metal composition within BDC-based MOFs. The comparison shows that the trivalent CoCuNi-BDC/NF electrode exhibits the highest specific capacitance among all reported MOFs, which indicates that the coexistence of multiple redox-active metal centers enhances charge storage. This improvement can be attributed to synergistic faradaic reactions that arises from the overlapping redox couples (Co^{2+}/Co^{3+}, Cu^{2+}/Cu^{+}, and Ni^{2+}/Ni^{3+}), as it increases the density of electrochemically active sites and promotes rapid surface redox processes characteristic of pseudocapacitive behavior. Similarly Bimetallic MOF system such as Fe/Ni-BDC also exhibited a higher capacitance than monometallic MOFs, which indicated the role of mixed-metal coordination environments in improving redox accessibility and electronic pathways. On the contrary, the monometallic MOFs such as Co-BDC and Mn-BDC show comparatively lower capacitance, which indicates the availability of fewer available redox sites which make the MOFs less conductive.

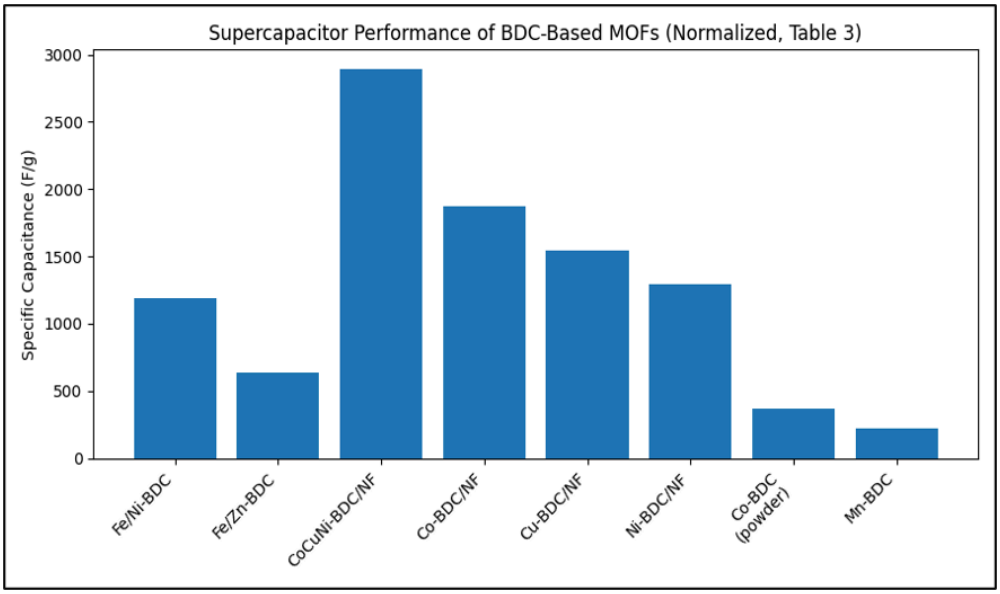

Figure 1 Comparative bar chart highlighting supercapacitor performance of BDC-based MOFs for different metal centers

The stability trends have been illustrated in Figure 2 which shows inverse relation between capacitance and long term cyclic retention. Here, monometallic MOFs show higher retention values which suggest that they had great structural stability during repeated charge-discharge processes. On the other hand, trimetallic systems even though has shown superior capacitance values but has reduced retention. It is likely due to increased structural complexity and mechanical stress induced by repeated redox cycling across multiple metal centers. This arises the need of such material which can be conductive and at the same time is stable.

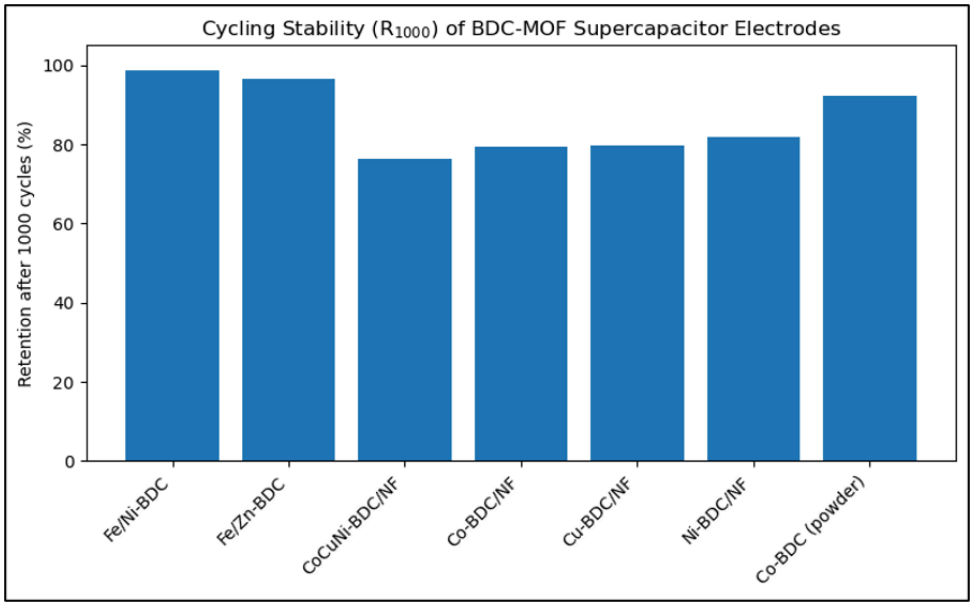

For Lithium-ion Batteries

The normalization strategy employed for the data set of Lithium-ion battery is to normalize the experimental values to common power density of 100 mA/g using following formula

$$\textbf{Capacity}_{100} = \textbf{Reported Capacity} \times \left(\frac{\boldsymbol{j}_{\textbf{reported}}}{\textbf{100}}\right)^{-0.25}$$

where $\boldsymbol{Capacity}_{100}$ represents the normalized specific capacity at 100 mA g^{-1}, ***Reported Capacity*** is the experimentally measured capacity, and $\boldsymbol{j}_{\textbf{reported}}$ is the applied current density. The exponent of −0.25 follows the general form of Peukert-type rate-capability relationships used for lithium-ion cells (e.g., Doerffel & Sharkh, J. Power Sources, 2006, 155(2), 395–400), and was applied here as an empirical approximation of the rate-capability trend common to the compared materials. Because rate capability is material- and mechanism-dependent, applying a single fixed exponent across chemically distinct Mn-, Co-, and Fe-based MOFs introduces uncertainty, and the rankings in Table 4 and Figure 3 should be interpreted with this caveat in mind. Table 4 is showing the normalized dataset for lithium-ion batteries. This dataset has been used to make comparison, and the plots have been made using python.

Table 4: Normalized data for Lithium-ion batteries

MOF System	Normalized Capacity (mAh g^{-1} @ 100 mA/g)	Ranking
Mn-1,4-BDC@200	**974**	Best overall
$Co_2(OH)_2BDC$	**773.5**	strong performance
Mn-1,4-BDC	**725.2**	good but lower than activated

Fe-MOF/RGO (5%)	**597**	graphene improved rate capability
Fe-MOF	**526.6**	moderate
Fe-MOF/RGO (10%)	**502.5**	lowest among Fe-based

The comparative bar chart (Figure 3) which has been made using the normalized dataset (Table 4) highlights a strong dependence of specific capacitance on metal composition within BDC-based MOFs. Among all reported systems, **thermally activated Mn-1,4-BDC@200** shows the highest normalized capacity, which indicate the significance of structural activation as it has enhanced lithium-ion storage. The improvement in performance is because of the increased surface area, improved pore accessibility, and reduced charge-transfer resistance, all of these factors have collectively facilitate faster lithium-ion diffusion, thus utilizing redox-active Mn centers more effectively. **$Co_2(OH)_2$BDC** demonstrates strong and stable lithium-storage performance, ranking second among the studied materials. This performance can be associated with the favourable redox kinetics of cobalt, moreover the robust framework also accommodates repeated lithiation and delithiation processes without major degradation of the structure. On the contrary, untreated Mn-1,4-BDC shows lower capacity than its thermally activated counterpart, which emphasizes the post-synthetic modification importance in optimizing the performance of MOF-based anodes. Fe-based MOFs show moderate normalized capacity, which indicates their low electronic conductivity, however when reduced graphene oxide is added in the MOF, it leads to performance enhancement, as observed for Fe-MOF/RGO (5%). The conductive graphene network improves electron transport and reduces polarization during cycling. When the graphene is used in higher amount (10%), the capacity does not further increase, which suggested that it may dilute the active material which may limit the accessibility of lithium-ion, thus the performance is not improved significantly.

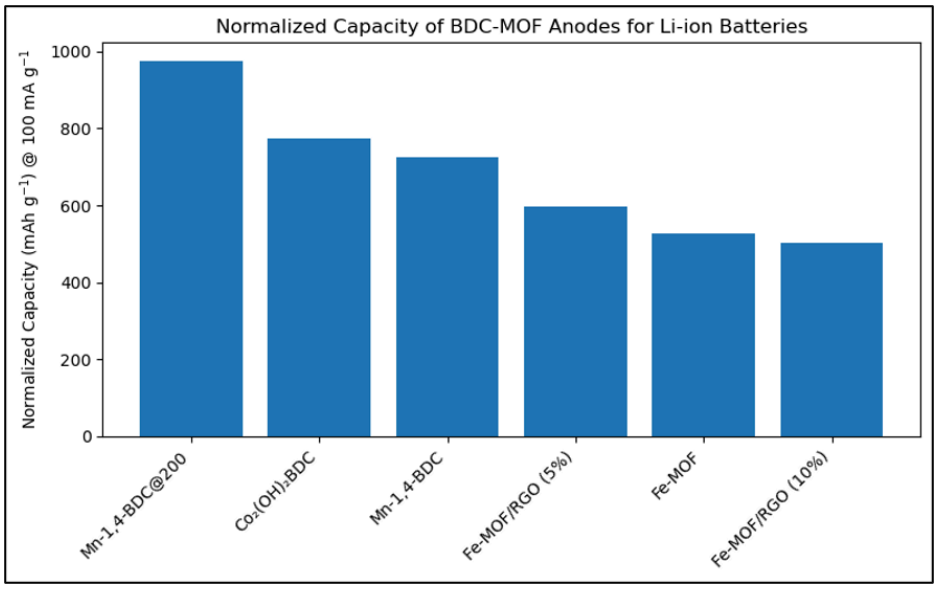

Figure 3 Bar Chart showing normalized capacity of BDC-MOF Anodes for Li-ion batteries

CONCLUSION

This comparative analysis establishes that the identity of the transition metal centre in BDC-based MOFs fundamentally determines electrochemical performance characteristics for energy storage applications. Since each material compared in this review was drawn from a single literature source with its own synthesis route, electrolyte, and electrode configuration, this trend should be read as a strong association rather than as fully isolating the effect of the metal centre independent of the ligand framework and testing conditions. Several key relationships emerge from this systematic comparison. First, incorporating multiple transition metal centres generates synergistic redox activity that substantially elevates specific capacitance in supercapacitor applications, with trimetallic CoCuNi-BDC/NF outperforming all monometallic analogues. However, this enhanced charge storage capacity introduces structural complexity that compromises long-term cycling stability, revealing an inherent trade-off between instantaneous performance and operational durability. Second, in lithium-ion battery systems, metal centre selection and post-synthetic activation together dictate reversible capacity, with thermally treated manganese-based frameworks achieving superior lithium storage through improved electronic accessibility and reduced interfacial resistance. Third, iron-based MOFs, despite favourable redox properties, require strategic integration of conductive additives such as graphene to compensate for poor intrinsic conductivity, a limitation that does not affect cobalt or nickel analogues to the same degree. These observations carry important implications for rational electrode design. Rather than pursuing universal optimization, researchers should match metal centre selection to specific application requirements. The strategic selection and combination of metal nodes, guided by the relationships established in this review, offers a direct path toward MOF electrodes optimized for next-generation electrochemical energy storage devices.

Limitations: Each material summarized in Tables 1 and 2 was drawn from a single literature source, and these sources differ from one another in synthesis route, electrolyte, and electrode configuration (some electrodes are powder-based and tested in a three-electrode cell, while others are grown directly on nickel foam). Because these variables are confounded with metal-centre identity across the compared studies, the performance trends reported here should be interpreted as associations observed across the literature rather than as a controlled, single-study comparison. Future work directly synthesizing and testing multiple metal centres under identical conditions with the same BDC ligand would allow the effect of metal-centre identity to be isolated more rigorously.

REFERENCES

1. Radwan, A., et al., *Design Engineering, Synthesis Protocols, and Energy Applications of MOF-Derived Electrocatalysts.* Nano-Micro Letters, 2021. **13**(1): p. 132.
2. Inderwildi, O., et al., *The impact of intelligent cyber-physical systems on the decarbonization of energy.* Energy & Environmental Science, 2020. **13**(3): p. 744-771.
3. Qian, Z., et al., *A review and discussion of decomposition-based hybrid models for wind energy forecasting applications.* Applied Energy, 2019. **235**: p. 939-953.

4. Wang, H., et al., *Metal-Organic Frameworks for Energy Applications.* Chem, 2017. **2**(1): p. 52-80.
5. Adegoke, K.A., et al., *Iron-based metal–organic frameworks and derivatives for electrochemical energy storage and conversion.* Coordination Chemistry Reviews, 2024. **517**: p. 215959.
6. Wei, D., et al., *Recent progress on construction and applications of metal-organic frameworks-based materials for lithium-ion batteries and supercapacitors.* Carbon Neutralization, 2024. **3**(3): p. 396-414.
7. Shakeel, M., et al., *Layered by layered Ni-Mn-LDH/g-C3N4 nanohybrid for multi-purpose photo/electrocatalysis: Morphology controlled strategy for effective charge carriers separation.* Applied Catalysis B: Environmental, 2019. **242**: p. 485-498.
8. Shakeel, M., et al., *In Situ Fabrication of Foamed Titania Carbon Nitride Nanocomposite and Its Synergetic Visible-Light Photocatalytic Performance.* Industrial & Engineering Chemistry Research, 2018. **57**(24): p. 8152-8159.
9. Arif, M., et al., *Coupling of Bifunctional CoMn-Layered Double Hydroxide@Graphitic C3N4 Nanohybrids towards Efficient Photoelectrochemical Overall Water Splitting.* Chemistry – An Asian Journal, 2018. **13**(8): p. 1045-1052.
10. Shakeel, M., et al., *Hollow mesoporous architecture: A high performance Bi-functional photoelectrocatalyst for overall water splitting.* Electrochimica Acta, 2018. **268**: p. 163-172.
11. Mehtab, T., et al., *Metal-organic frameworks for energy storage devices: Batteries and supercapacitors.* Journal of Energy Storage, 2019. **21**: p. 632-646.
12. Miller, E.E., Y. Hua, and F.H. Tezel, *Materials for energy storage: Review of electrode materials and methods of increasing capacitance for supercapacitors.* Journal of Energy Storage, 2018. **20**: p. 30-40.
13. Dubal, D.P., et al., *Towards flexible solid-state supercapacitors for smart and wearable electronics.* Chemical Society Reviews, 2018. **47**(6): p. 2065-2129.
14. Ibrahim Abouelamaiem, D., et al., *New insights into the electrochemical behaviour of porous carbon electrodes for supercapacitors.* Journal of Energy Storage, 2018. **19**: p. 337-347.
15. Schmidt, D., M. Kamlah, and V. Knoblauch, *Highly densified NCM-cathodes for high energy Li-ion batteries: Microstructural evolution during densification and its influence on the performance of the electrodes.* Journal of Energy Storage, 2018. **17**: p. 213-223.
16. Whittingham, M.S., *Ultimate Limits to Intercalation Reactions for Lithium Batteries.* Chemical Reviews, 2014. **114**(23): p. 11414-11443.
17. Niu, L., et al., *Conductive metal–organic frameworks for supercapacitors.* Advanced materials, 2022. **34**(52): p. 2200999.
18. Hong, C.N., et al., *Metal-organic frameworks for fast electrochemical energy storage: Mechanisms and opportunities.* Chem, 2023. **9**(4): p. 798-822.
19. Fujie, K. and H. Kitagawa, *Ionic liquid transported into metal–organic frameworks.* Coordination Chemistry Reviews, 2016. **307**: p. 382-390.
20. Hu, Y., et al., *Design principles of MOF-related materials for highly stable metal anodes in secondary metal-based batteries.* Materials Today Energy, 2021. **19**: p. 100608.
21. Simon, P. and Y. Gogotsi, *Perspectives for electrochemical capacitors and related devices.* Nature materials, 2020. **19**(11): p. 1151-1163.

22. Abakumov, A.M., et al., *Solid state chemistry for developing better metal-ion batteries.* Nature Communications, 2020. **11**(1): p. 4976.
23. Lukatskaya, M.R., B. Dunn, and Y. Gogotsi, *Multidimensional materials and device architectures for future hybrid energy storage.* Nature communications, 2016. **7**(1): p. 12647.
24. Zeggai, F.z., et al., *Investigation of Metal-Organic Frameworks (MOFs): Synthesis, Properties, and Applications - An In-Depth Review.* Chemical Physics Impact, 2025. **10**: p. 100864.
25. Liang, Y., et al., *Organo-macrocycle-containing hierarchical metal–organic frameworks and cages: design, structures, and applications.* Chemical Society Reviews, 2022. **51**(19): p. 8378-8405.
26. Dutta, A., et al., *Multicomponent isoreticular metal-organic frameworks: Principles, current status and challenges.* Coordination Chemistry Reviews, 2021. **445**: p. 214074.
27. Sandhu, Z.A., et al., *Metal–organic frameworks for next-generation energy storage devices; a systematic review.* Materials Advances, 2024. **5**(1): p. 30-50.
28. Liang, Y., Z. Tao, and J. Chen, *Organic Electrode Materials for Rechargeable Lithium Batteries.* Advanced Energy Materials, 2012. **2**(7): p. 742-769.
29. Liu, B., et al., *Metal–organic framework (MOF) as a template for syntheses of nanoporous carbons as electrode materials for supercapacitor.* Carbon, 2010. **48**(2): p. 456-463.
30. Morozan, A. and F. Jaouen, *Metal organic frameworks for electrochemical applications.* Energy & Environmental Science, 2012. **5**(11): p. 9269-9290.
31. Hu, Y.Y., et al., *Design principles of MOF-related materials for highly stable metal anodes in secondary metal-based batteries.* Materials Today Energy, 2021. **19**: p. 100608.
32. Zhang, R., et al., *Recent electrochemical-energy-storage applications of metal–organic frameworks featuring iron-series elements (Fe, Co, and Ni).* Journal of Energy Storage, 2023. **65**: p. 107217.
33. Sun, L., et al., *Million-fold electrical conductivity enhancement in Fe2 (DEBDC) versus Mn2 (DEBDC)(E= S, O).* Journal of the American Chemical Society, 2015. **137**(19): p. 6164-6167.
34. Cavka, J.H., et al., *A new zirconium inorganic building brick forming metal organic frameworks with exceptional stability.* Journal of the American Chemical Society, 2008. **130**(42): p. 13850-13851.
35. Sheberla, D., et al., *High electrical conductivity in Ni3 (2, 3, 6, 7, 10, 11-hexaiminotriphenylene) 2, a semiconducting metal–organic graphene analogue.* Journal of the American Chemical Society, 2014. **136**(25): p. 8859-8862.
36. Dou, J.-H., et al., *Signature of metallic behavior in the metal–organic frameworks M3 (hexaiminobenzene) 2 (M= Ni, Cu).* Journal of the American Chemical Society, 2017. **139**(39): p. 13608-13611.
37. Xie, L.S., G. Skorupskii, and M. Dinca, *Electrically conductive metal–organic frameworks.* Chemical reviews, 2020. **120**(16): p. 8536-8580.
38. Nath, A., K. Asha, and S. Mandal, *Conductive Metal‐Organic Frameworks: Electronic Structure and Electrochemical Applications.* Chemistry–A European Journal, 2021. **27**(45): p. 11482-11538.
39. Sun, T., et al., *Identifying MOFs for electrochemical energy storage via density functional theory and machine learning.* npj Computational Materials, 2025. **11**(1): p. 90.
40. Sun, L., M.G. Campbell, and M. Dincă, *Electrically conductive porous metal–organic frameworks.* Angewandte Chemie International Edition, 2016. **55**(11): p. 3566-3579.

41. Skorupskii, G., et al., *Efficient and tunable one-dimensional charge transport in layered lanthanide metal–organic frameworks.* Nature chemistry, 2020. **12**(2): p. 131-136.
42. Yang, M., et al., *Two‐Dimensional Conjugated Metal–Organic Frameworks with a Ring‐in‐Ring Topology and High Electrical Conductance.* Angewandte Chemie International Edition, 2024. **63**(26): p. e202405333.
43. Zhang, J., et al., *Wavy two-dimensional conjugated metal–organic framework with metallic charge transport.* Journal of the American Chemical Society, 2023. **145**(43): p. 23630-23638.
44. Baumann, A.E., et al., *Metal-organic framework functionalization and design strategies for advanced electrochemical energy storage devices.* Communications Chemistry, 2019. **2**(1): p. 86.
45. Zhang, W., et al., *One-Step Facile Solvothermal Synthesis of Copper Ferrite–Graphene Composite as a High-Performance Supercapacitor Material.* ACS Applied Materials & Interfaces, 2015. **7**(4): p. 2404-2414.
46. Zhou, M., et al., *One-pot construction of three dimensional CoMoO 4/Co 3 O 4 hybrid nanostructures and their application in supercapacitors.* Journal of Materials Chemistry A, 2015. **3**(42): p. 21201-21210.
47. Tomar, S. and V.K. Singh, *Cobalt and copper-based metal-organic frameworks synthesis and their supercapacitor application.* Journal of Electrochemical Science and Engineering, 2024. **14**(2): p. 163-175.
48. Sundriyal, S., S. Mishra, and A. Deep, *Study of manganese-1, 4-benzenedicarboxylate metal organic framework electrodes based solid state symmetrical supercapacitor.* Energy Procedia, 2019. **158**: p. 5817-5824.
49. Nivetha, R., et al., *Two-dimensional bimetallic Fe/M-(Ni, Zn, Co and Cu) metal organic framework as efficient and stable electrodes for overall water splitting and supercapacitor applications.* Journal of Energy Storage, 2023. **61**: p. 106702.
50. Mohd Zain, N.K., et al., *Direct growth of triple cation metal–organic framework on a metal substrate for electrochemical energy storage.* Industrial & Engineering Chemistry Research, 2018. **58**(2): p. 665-674.
51. Goodenough, J.B., *Electrochemical energy storage in a sustainable modern society.* Energy & Environmental Science, 2014. **7**(1): p. 14-18.
52. Tarascon, J.M., *Towards sustainable and renewable systems for electrochemical energy storage.* ChemSusChem: Chemistry & Sustainability Energy & Materials, 2008. **1**(8‐9): p. 777-779.
53. Xu, Y., et al., *Metal-organic frameworks for direct electrochemical applications.* Coordination Chemistry Reviews, 2018. **376**: p. 292-318.
54. Goodenough, J.B. and Y. Kim, *Challenges for Rechargeable Li Batteries.* Chemistry of Materials, 2010. **22**(3): p. 587-603.
55. Hu, H., et al., *A thermally activated manganese 1, 4-benzenedicarboxylate metal organic framework with high anodic capability for Li-ion batteries.* New Journal of Chemistry, 2016. **40**(11): p. 9746-9752.
56. Gou, L., et al., *One-pot synthesis of a metal–organic framework as an anode for Li-ion batteries with improved capacity and cycling stability.* Journal of Solid State Chemistry, 2014. **210**(1): p. 121-124.

57. Combelles, C., et al., *Design of electrode materials for lithium-ion batteries: the example of metal–organic frameworks.* The Journal of Physical Chemistry C, 2010. **114**(20): p. 9518-9527.
58. Fateeva, A., et al., *Synthesis, structure, characterization, and redox properties of the porous MIL‐68 (Fe) solid*. 2010, Wiley Online Library.
59. Férey, G., et al., *Mixed‐valence Li/Fe‐based metal–organic frameworks with both reversible redox and sorption properties.* Angewandte Chemie International Edition, 2007. **46**(18): p. 3259-3263.
60. Wiers, B.M., et al., *A solid lithium electrolyte via addition of lithium isopropoxide to a metal–organic framework with open metal sites.* Journal of the American Chemical Society, 2011. **133**(37): p. 14522-14525.
61. Shin, J., et al., *MIL-101 (Fe) as a lithium-ion battery electrode material: a relaxation and intercalation mechanism during lithium insertion.* Journal of Materials Chemistry A, 2015. **3**(8): p. 4738-4744.
62. Zhen, M., et al., *Reduced Graphene Oxide‐Supported TiO2 Fiber Bundles with Mesostructures as Anode Materials for Lithium‐Ion Batteries.* Chemistry–A European Journal, 2015. **21**(41): p. 14454-14459.
63. Jin, Y., et al., *Facile synthesis of Fe-MOF/RGO and its application as a high performance anode in lithium-ion batteries.* RSC advances, 2016. **6**(36): p. 30763-30768.